frontiers | Frontiers in Earth Science

BRIEF RESEARCH REPORT
published: 08 July 2022
doi: 10.3389/feart.2022.878318

Chronology of Glacial Advances and Deglaciation in the Encierro River Valley (29° Lat. S), Southern Atacama Desert, Based on Geomorphological Mapping and Cosmogenic ^{10}Be Exposure Ages

G. Aguilar[1]*, *R. Riquelme*[2], *P. Lohse*[2], *A. Cabré*[3] and *J.-L. García*[4]

[1]Advanced Mining Technology Center (AMTC), Facultad de Ciencias Físicas y Matemáticas, Universidad de Chile, Santiago, Chile, [2]Departamento de Ciencias Geológicas, Universidad Católica del Norte, Antofagasta, Chile, [3]Géosciences Environnement Toulouse (GET), CNRS/IRD/CNES/UPS, Toulouse, France, [4]Instituto de Geografía, Pontificia Universidad Católica de Chile, Santiago, Chile

OPEN ACCESS

Edited by:
Daniel Nývlt,
Masaryk University, Czechia

Reviewed by:
Henry Patton,
UiT The Arctic University of Norway, Norway
Naki Akçar,
University of Bern, Switzerland

***Correspondence:**
G. Aguilar
german.aguilar@amtc.uchile.cl

Specialty section:
This article was submitted to Quaternary Science, Geomorphology and Paleoenvironment, a section of the journal Frontiers in Earth Science

Received: 17 February 2022
Accepted: 30 May 2022
Published: 08 July 2022

Citation:
Aguilar G, Riquelme R, Lohse P, Cabré A and García J-L (2022) Chronology of Glacial Advances and Deglaciation in the Encierro River Valley (29° Lat. S), Southern Atacama Desert, Based on Geomorphological Mapping and Cosmogenic ^{10}Be Exposure Ages. Front. Earth Sci. 10:878318. doi: 10.3389/feart.2022.878318

The high mountain segments of the valleys of the southernmost Atacama Desert of Chile present Late Quaternary glacial landforms that developed in already incised valleys. Glacier advances and deglaciation have left a geomorphic imprint in the southernmost Atacama Desert. In this work, the glacial landforms of the Encierro River Valley (29.1°S–69.9°W) have been revisited and new detailed geomorphological mapping is provided. This work also includes new ^{10}Be exposure ages from moraine boulders and one age from an ice-molded bedrock surface. The former glacier of the El Encierro valley extended 16 km down the valley during the last local glacial maximum recorded by a terminal moraine (ENC 1a) with an exposure age of ~40 ka. Four inboard moraine arcs were deposited upstream in telescopic patterns (ENC 1b–d), whose exposure ages range between ~25 and ~33 ka (ENC 1d). Exposure ages between ~17–24 ka on lateral moraines (ENC 1L) developed during the later ice recession of the ENC 1 drift. Thus, the ice mostly disappeared in the main valley before ~18 ka, as is also supported by the exposure age obtained from an ice-molded bedrock surface. Seven kilometers up the valley from the ENC 1, the ENC 2a–d moraine arcs correspond to a small ice advance by ~17–20 ka. The last glacial advance (ENC 2), which occurred after deglaciation of the last local glacial maximum (ENC 1), coincides with the start of the Heinrich Stadial Event 1 (HS1; 18–14.5 ka), which is thought to play a direct role in the last glacial termination in the Andes.

Keywords: Atacama desert, glacial termination, Andes cordillera, deglaciation age, ^{10}Be exposure ages

1 INTRODUCTION

The southern Atacama Desert (27–30°S) is a climatic transitional region between the tropics and the extratropic source of moisture. As such, it is not certain whether the influence of one, or the other, or both, controls glacier and climate dynamics in the region (e.g., Zech et al., 2006). There is still debate about which source of moisture was responsible for driving glacier dynamics and the associated

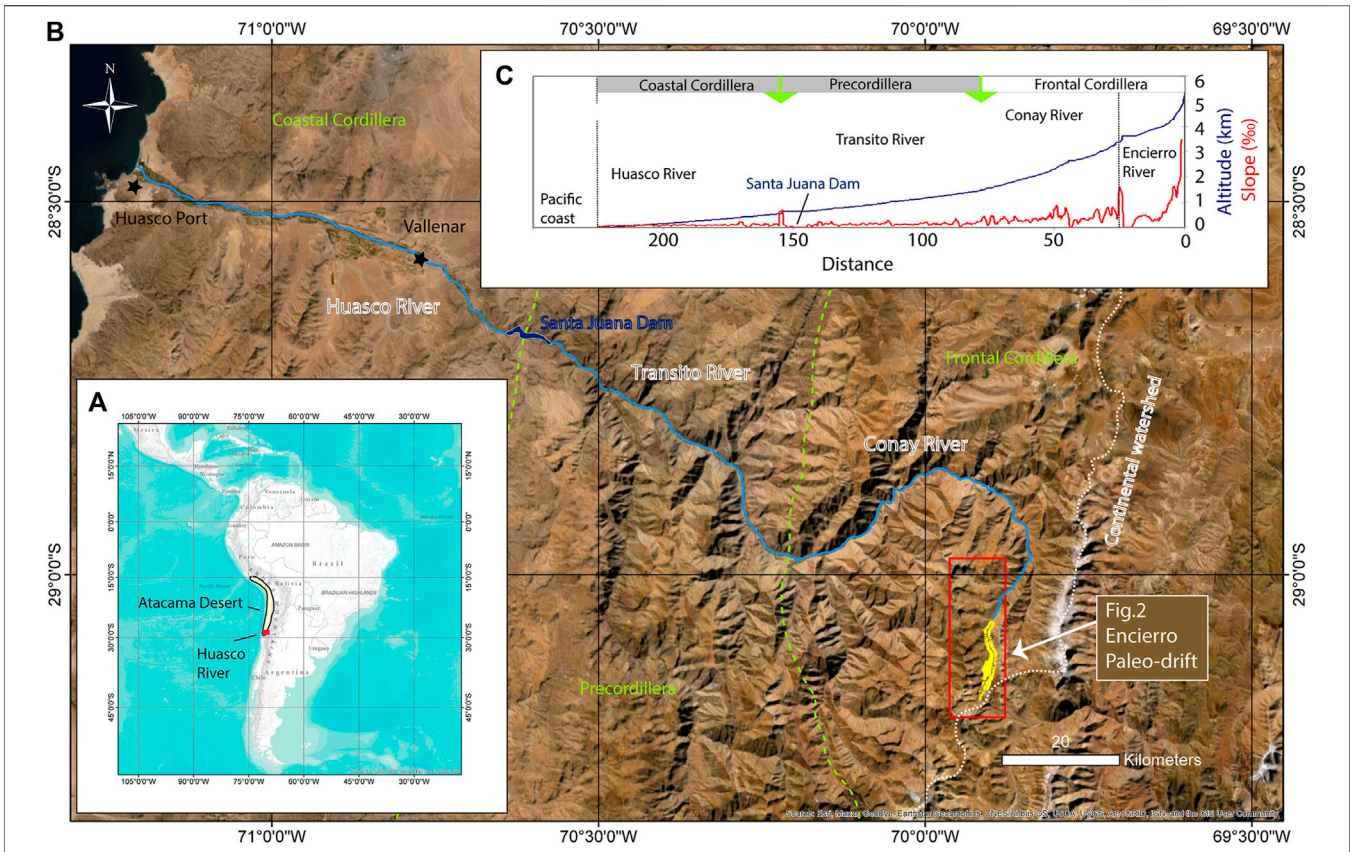

FIGURE 1 | Location map of the Encierro Valley in the Southern Atacama Desert. **(A)** Inset map with study area in South America. **(B)** DEM and morphostructural segments of the western slopes of the Andes. **(C)** Longitudinal Encierro-Huasco River topographic profile between the Encierro Valley and Pacific Coast.

hydrographic evolution during the Local Last Glacial Maximum (LLGM) and termination (e.g., Ammann et al., 2001). Therefore, determining the former geographic influence of extratropical winter westerly and/or tropical easterly wind belts in this region remains a major open question. The limited dated records in the southern Atacama region still hinder reaching firm conclusions. Veit (1993), Veit (1996), and Ammann et al. (2001) pointed to extra-tropical westerlies as responsible for driving former ice/climate fluctuations in this part of the Andes. Jenny and Kammer (1996) remark on the tropical influence through the easterlies origination in the Amazonian and the Chaco Region (e.g., D'Arcy et al., 2019), whereas Zech et al. (2017) suggest that both seasonal circulation systems were operating together. These interpretations are based on geomorphological and geochronological studies of landforms sculpted by ancient glaciers, but often lack a holistic view of the evolution of arid landscapes.

One of the valleys in the Atacama Desert where glacial landforms which originated from former glacial advances are preserved is El Encierro valley. Pioneer studies carried out by Veit (1993), Veit (1996), Jenny and Kammer (1996), and Grosjean et al. (1998) suggest that the El Encierro River Valley (ERV, 29.1°S–69.9°W, 3,750–4,150 m asl, **Figure 1**) was occupied by mountain glaciers that extended several kilometers during the LLGM. More recently, investigations by Zech et al. (2006) and Zech et al. (2017) have dated ^{10}Be the outer moraine (MII) to 20–22 ka during the LLGM inboard moraines (MIII–MV) been interpreted as recessional glacial re-advances dated between 16 and 18 ka. Zech et al. (2017) suggest this glacial re-advance was related to the humid phase recorded in the tropical Andes known as the Central Andean Pluvial Event (CAPE; Latorre et al., 2006; Quade et al., 2008). With this evidence, these authors suggest that this glacial re-advance is linked to a tropical supply of moisture reaching the southern Atacama Desert (Zech et al., 2006; Zech et al., 2017).

This research report presents a geomorphological map and reports seven new cosmogenic ^{10}Be exposure ages obtained from boulders and an ice-molded bedrock surface in the paleo-drift of the ERV. The ERV is a tributary of the El Huasco River (**Figure 1**), one of the southern Atacama Desert's main Andean catchments where the geomorphological evolution associated with Late Pleistocene and Early Holocene hydro-climatic changes is remarkably well preserved. Based on our geomorphological mapping in the field, different glacial landforms were characterized and dated with ^{10}Be to reconstruct the former glacial advances and deglaciation. We include geomorphic interpretations and recalibrated ^{10}Be data from previous works in this valley (Jenny and Kammer, 1996; Grosjean et al., 1998; Zech et al., 2006). Finally, the results are discussed to provide an updated

perspective of understanding the spatio-temporal variability of the former El Encierro Glacier during the LLGM and the Pleistocene–Holocene transition.

2 METHODS

2.1 Geomorphological Mapping and Sampling

The identification and mapping of the different landforms of the ERV were carried out based on field observations, mapping over aerial photography from the 1997 aerofotogrammetric survey carried out by SAF (www.saf.cl) and using optical satellite imagery retrieved from different sources, including Bing, ESRI, and Google Earth. Six rock samples from the largest boulders located at the crest of moraines and one sample from ice-molded bedrock surface in the valley bottom were collected for subsequent dating by ^{10}Be concentrations in quartz using the sampling protocol described by Ivy-Ochs (1996). In the field, the shielding of cosmic radiation affecting the rock surfaces was calculated considering the topography of the valley by Brunton structural compass measurement of the surface elevation angle relative to the topography for 8 azimuths. Although the blocks are not exceptionally large, it was verified in the field that they have not been rotated considering imbrications with other blocks that indicate stability.

2.2 Analytical Procedures

The measurement of the ^{10}Be concentration was performed in the year 2008. The samples were crushed and sieved to obtain the 250–710 mm size fractions for analysis. The quartz mineral was separated (see quartz mass in Supplementary Data) and dissolved in a hot ultrasonic bath and/or on a shaking table using a combination of acids (HF, HCl, and HNO_3). The extraction and preparation of BeO targets were conducted at the University of Edinburgh's Cosmogenic Isotope Laboratory following procedures adapted from the methods of Bierman et al. (2002), Kohl and Nishiizumi (1992), and Ivy-Ochs (1996). The colloid containing the ^{10}Be concentrate was precipitated from the solution, which also contains approximately 1 mg of previously added ^{9}Be (see supplementary data). Finally, the ^{10}Be/^{9}Be ratios were measured using an accelerator mass spectrometer of the Scottish Universities Environment Research Centre (SUERC; https://www.suerc-cosmo.co.uk/). All measurements are standardized relative to 07KNSD (Nishiizumi et al., 2007).

Cosmogenic ^{10}Be exposure ages were calculated using the online CREp calculator (crep.crpg.cnrs-nancy.fr; Martin et al., 2016). They were computed using the scaling scheme Lal/Stone time dependent (Lal, 1991; Stone, 2000; Balco et al., 2008), with the ERA-40 (Uppala et al., 2005), the geomagnetic record of atmospheric ^{10}Be-based VDM (Muscheler, et al., 2005; Valet et al., 2005), and the production rates (4.17 at/gr/yr) calibrated by Martin et al. (2015) at Bolivian mountains (19°S and 3,800 m asl).

Calculation of topographic shielding was included considering the fieldwork measures by Brunton Compass and using the topographic shielding calculator of CRONUS-Earth online calculators (http://stoneage.ice-d.org/math/skyline/skyline_in.html). Age calculations consider an erosion rate of 0 mm/ka, as the percentage of variation per mm of erosion is only 1%, significantly less than the error associated with the ^{10}Be measurement. Additionally, 11 ^{10}Be exposure ages previously obtained by Zech et al. (2006) were recalculated using the same parameters. The ages published by Zech et al. (2006) consider much higher ^{10}Be production rates in quartz (5.25 at/gr/yr) that are not in agreement with the rates currently used for this region of the Andes (Martin et al., 2015).

3 RESULTS

The geomorphological map allows the recognition of two moraine systems (ENCs) with a telescopic plan-view of arc morphologies. The two-terminal moraines of these systems are situated at 16 (ENC 1a) and 9 km (ENC 2a) downstream of the catchment head.

In total, three ages were obtained in moraine boulders in the outermost system (ENC 1) and two in the internal system of moraines (ENC 2). An additional ^{10}Be sample was obtained from an ice-molded bedrock surface on the valley bottom in ENC 2 and also in a lateral moraine (ENC 1L) situated between ENC 1 and ENC 2. **Table 1** summarizes the characteristics of the sample, the measured ^{10}Be concentrations, the exposure ages, and the correlation with moraine stages defined by Zech et al. (2006) in view of their recalibrated and incorporated ages in this article. ^{10}Be exposure ages range between 39.1 ± 1.7 ka and 17.2 ± 0.8 ka, without considering one outlier of 193.7 ± 7.3 ka which is not considered in the following sections of this report.

Some boulders sitting on top of moraines have a length of up to 3 m along their main axis. Some of these boulders are partially buried and emerge a few tens of centimeters above the surface, so the possibility of a prior complete burial condition of them cannot be excluded. The same post-glacial conditions of burying could be assigned to the ^{10}Be-dated ice-molded bedrock surface. So, boulders and bedrock surface ages should be considered always as minimum ones.

Rock glaciers (RGs) cover large areas of the headwaters in the tributary valleys of ERV (**Figure 2**). Some of these RGs are still actively indicated with accumulations of boulders at their front. Although they are not the focus of this brief research report, RGs are mapped to highlight that the potential preservation of moraines of tributary glaciers has been compromised. The non-consolidated Neogene Gravels Units on the hillslopes of the ERV (12 Ma, Salazar and Coloma, 2016) are included (**Figure 2**) because its distribution was not available at the time of Zech et al. (2006) and are remains of the infilling history of the valley with fluvial processes.

3.1 Moraine System ENC 1

Moraine ridges are arranged with telescoping arc morphologies in plan-view at 3,650–3,750 m asl. (**Figure 2**). The external moraine of the arc (ENC 1a) is a degraded terminal moraine while the other four inboard moraine ridges are at 100–200 m from each other (ENC 1b–d). The terminal moraine represents the outermost limit of glacial deposits in the ERV and comprises the lowermost glacial drift mapped in this valley. The ENC 1 moraine ridges correspond to the S-II system defined by Jenny and Kammer (1996) and the M-II system defined by Grosjean et al. (1998). Grosjean's nomenclature

TABLE 1 | Sample information, the measured ^{10}Be concentrations in quartz and calculated ^{10}Be exposure age of this work (HPL) and recalculated from Zech et al. (2006) in the Encierro Valley (EE). A density of 2.7 g/cm^3 was considered for quartz. Detailed analytic results in supplementary digital materials.

Sample ID	Moraine System	Landform	LAT	LONG	Altitude (m)	Topographic Shielding	Concentrations (at/gr)	1σ (at/g)	Scaling Factor	Age (ka)	1σ (ka)
EE71	ENC 1a	Outer terminal moraine arc	−29.065	−69.901	3,678	0.988	1,47E+06	6,04E+07	9.32	39.1	1.7
HPL28	ENC 1d	Inner terminal moraine arc	−29.068	−69.904	3,696	0.981	7,20E+09	1,01E+08	9.7	193.7	7.3
HPL29	ENC 1d	Inner terminal moraine arc	−29.068	−69.904	3,670	0.981	9,65E+08	1,36E+07	9.16	26.4	0.9
HPL30	ENC 1d	Inner terminal moraine arc	−29.071	−69.905	3,699	0.981	1,16E+09	1,68E+07	9.4	31.0	1.5
EE62	ENC 1d	Inner terminal moraine arc	−29.068	−69.902	3,688	0.988	7,55E+05	3,17E+07	9.16	20.5	1.0
EE63	ENC 1d	Inner terminal moraine arc	−29.068	−69.902	3,684	0.988	5,30E+05	2,17E+07	8.69	15.1	0.7
HPL26	ENC 1L	Lateral moraine, eastern slopes	−29.110	−69.891	3,970	0.978	1,38E+09	2,50E+07	10.38	33.4	1.5
EE33	ENC 1L	Lateral moraine, western slopes	−29.109	−69.901	4,055	0.997	7,92E+05	3,25E+07	10.81	18.0	0.9
EE34	ENC 1L	Lateral moraine, western slopes	−29.110	−69.901	4,029	0.997	1,00E+06	5,93E+07	11.02	22.4	1.6
EE42	ENC 1L	Lateral moraine, western slopes	−29.102	−69.901	3,955	0.997	8,38E+05	4,02E+07	10.45	19.7	1.1
EE51	ENC 1L	Lateral moraine, western slopes	−29.092	−69.907	3,900	0.984	8,98E+05	3,86E+07	10.31	21.7	1.2
EE11	ENC 2a	Outer terminal moraine arc	−29.133	−69.898	3,971	0.997	8,01E+05	3,28E+07	10.44	18.9	0.9
EE12	ENC 2a	Outer terminal moraine arc	−29.133	−69.898	3,971	0.997	7,83E+05	2,90E+07	10.41	18.5	0.9
EE22	ENC 2L	Lateral moraine on tributary	−29.125	−69.904	3,998	0.997	7,32E+05	2,71E+07	10.43	17.2	0.8
EE24	ENC 2L	Lateral moraine on tributary	−29.125	−69.905	3,994	0.997	7,64E+05	3,21E+07	10.48	17.9	0.9
HPL31	ENC 2 mb	Ice-molded bedrock	−29.155	−69.913	4,124	0.967	8,39E+08	1,27E+07	11.28	18.8	0.7
HPL07	ENC 2d	Inner recessional moraine ridge	−29.162	−69.916	4,153	0.967	8,26E+08	1,34E+07	11.39	18.4	0.7
HPL33	ENC 2d	Inner recessional moraine ridge	−29.162	−69.916	4,153	0.967	7,76E+08	1,46E+07	11.29	17.4	0.7

was the nomenclature used by Zech et al. (2006) with their ^{10}Be exposure ages.

The published exposures ^{10}Be ages of Zech et al. (2006) are recalculated here to 39.1 ± 1.7 ka (EE71) in ENC 1a and 20.5 ± 1.0 ka (EE62) and 15.1 ± 0.7 ka (EE63) in ENC 1d. There is not sufficient replicability in the ages considering the intersect of its probability (**Figure 3A**). Two new ^{10}Be exposure ages provided in this work are 26.4 ± 0.9 ka (HPL-29) and 31.0 ± 1.5 ka (HPL-30) for the well-preserved inboard moraine ENC 1d (**Figure 2**).

Only one age of 33.4 ± 1.5 (HPL-26) was obtained from the lateral moraine (ENC 1L) on the eastern hillslope that can be tracked for about 7 km upstream of the external moraine of the arc ENC 1a (**Figure 2B**, **Figure 4AB**). This lateral moraine (ENC 1L) correlates geomorphologically with the frontal moraine ENC 1d (33–25 Ka). This is an older age in relation to four ages (EE33, EE34, EE42, and EE51; **Figure 4A**) measured by Zech et al. (2006) on the lateral moraines ENC 1L of the western hillslopes with an intersect ages between 17 and 24 ka considering error in samples (**Figure 3B**).

3.2 Moraine System ENC 2

Between seven and 10 km up-valley from ENC 1a, four well-preserved moraine ridges were identified in plan-view telescoping arc morphologies between 3,900 m a.s.l. and 4,100 m a.s.l. (**Figure 2**). These moraine ridges define the glacial front of the system ENC 2. Zech et al. (2006) published exposure ^{10}Be ages recalculated here with ages of 18.9 ± 0.9 ka (EE11) and 18.5 ± 0.9 ka (EE12) in the external terminal moraine (ENC 2a). A lateral moraine (ENC 2L) in a tributary valley located downstream is dated 17.2 ± 0.8 ka (EE22) and 17.9 ± 0.9 (EE24) by Zech et al. (2006). This lateral moraine was interpreted by Zech et al. (2006) as a recessional moraine.

The two ^{10}Be exposure ages provided in this work are 17.4 ± 0.7 ka (HPL-33) and 18.4 ka ± 0.7 ka (HPL-07) for the upstream inboard recessional moraine ridge (ENC 2d), and an age of 18.8 ± 0.7 ka (HPL-31) for an ice-molded granitic bedrock surface of valley bottom 1-km downstream of ENC 2d. Moraine ridge ENC 2d and the erosional glacial landforms are not included in previous geomorphological maps of the ERV. They are mapped and dated here for the first time. Intersect ages considering the error of all samples of the ENC 2 system are between 17 and 19 ka (**Figure 3C**).

4 INTERPRETATIONS

Tills fill the valley along 16 km as low as 3,650 m a.s.l., while a preserved Neogene Gravel Units formed by non-consolidated

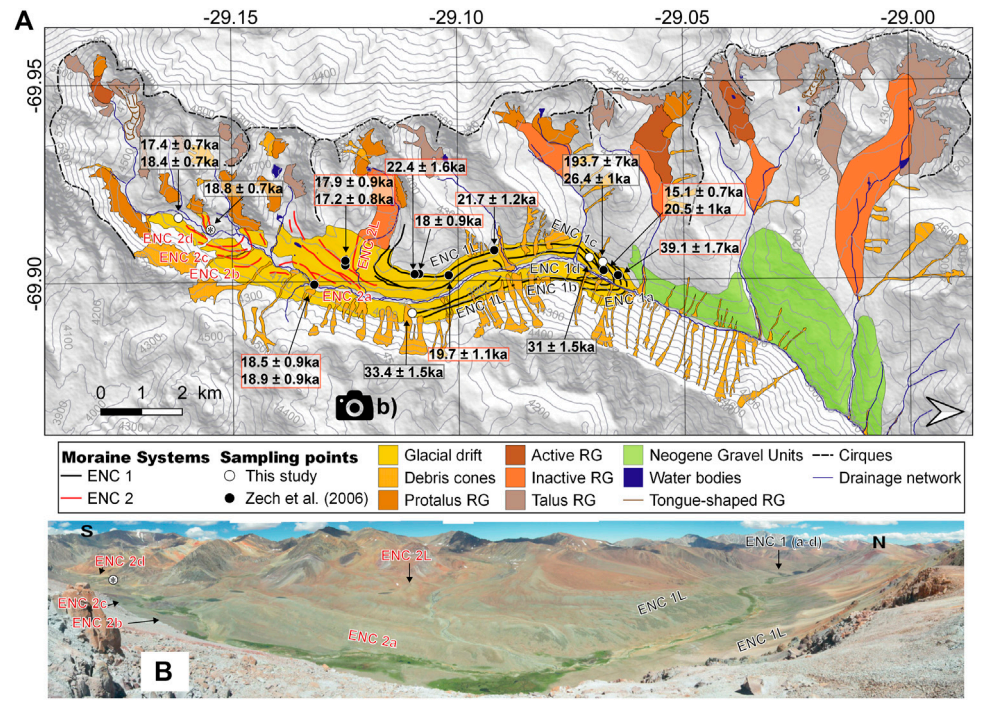

FIGURE 2 | (A) Geomorphological map showing ^{10}Be exposure ages of this study (white solid circles) and recalculated from Zech et al. (2006) (black solid circles). The sample from the ice-molded bedrock surface is highlighted within the sampling points of figure A with an *. RG: rock glacier. **(B)** Photograph toward the west taken from the east slope of the ERV showing the distribution of moraine ridges mapped in panel 2A.

polymictic alluvial deposits are identified downstream on the hillslopes of the ERV (**Figure 2**; Salazar and Coloma, 2016; Rossel et al., 2018). In the ERV, these Neogene Gravel Units hanging on valley slopes mapped in works from the Chilean Geological Survey (Salazar and Coloma, 2016) and in Miocene tectonostratigraphic Andean interpretations (Rossel et al., 2018) have been dated with interlocked tuff levels indicating a minimum age of 12 Ma. These recently published observations deny the interpretations that considered these deposits as till-forming moraines (MI) associated with a pre-LLGM glacial advance that reached 3,450 m a.s.l. and distant almost 20 km from the glacial cirque (Jenny and Kammer, 1996; Grosjean et al., 1998).

The presence of these Neogene gravels in the ERV identified by Salazar and Coloma (2016) suggests that the tills are in part composed of reworked Neogene gravels and so, the glacial forms could be in part the result of the redistribution of former non-consolidated alluvial deposits during glacial advances. The lateral moraines preserved on the hillslopes of ERV occur at a similar altitude as the non-consolidated Neogene gravels in relation to the valley floor and thus might have led to misinterpretations in the past. Thus, moraines distributions are indicators of the lateral limits of the glaciers that occupied the valley, but the supply of sediments was controlled, at least in part, by the Neogene gravels. This implies that particular attention should be paid when interpreting the spatial extent of glacial advances in arid valleys with well-preserved and thick ancient alluvial gravel successions.

In total, nine out of eleven ages of ENC 1 give a range between 40–25 ka (4 samples) and 18–22 (5 samples) (**Figure 2**, **Figure 3**), whereas one sample is younger (15 ka) and another is an outlier (193.7 ± 7.3). Thus, the oldest geomorphological evidence of glaciations in the ERV is the arc related to ENC 1, which represents the LLGM. The LLGM in the ERV was punctuated by several glacial advances (ENC 1a–d), which extended 16–14 km from the headwaters and down to 3,650–3,750 m a.s.l. In that sense, and based on the available data and supported by the preference of depositional ages assignment to the oldest-one-model (e.g., D'Arcy et al., 2019), we define that the external terminal moraine arc ENC 1a and the inner terminal moraine arc ENC 1d were deposited by full glacial conditions during ice expansions at ~40 ka and 33–25 ka respectively. Glacial advances recorded in this valley have been reported in other nearby valleys of the Atacama Desert (e.g., Zech et al., 2011; Zech et al., 2017) and on the eastern slope of the Andes at similar latitudes (e.g., D'Arcy et al., 2019, 27°S).

Overall, five ages from moraine boulders on ENC 1 system are between 17–24: Four ages on a lateral moraine ENC 1L (EE33, EE34, EE42, and EE51) in the western slope of the ERV, and one on the inner terminal moraine arc ENC 1d (EE62). We interpret that these ages constrain the glacial recession or the paraglacial readjustment of moraines after the deglaciation (**Figure 3**). In fact, the tributaries situated in the west developed several rock glaciers that filled tributary valleys and reached the trunk valley after the deglaciation. The ridges on the eastern slope that avoid the influence of rock glaciers are dated at 33.4 ± 1.5 (HPL-26) and

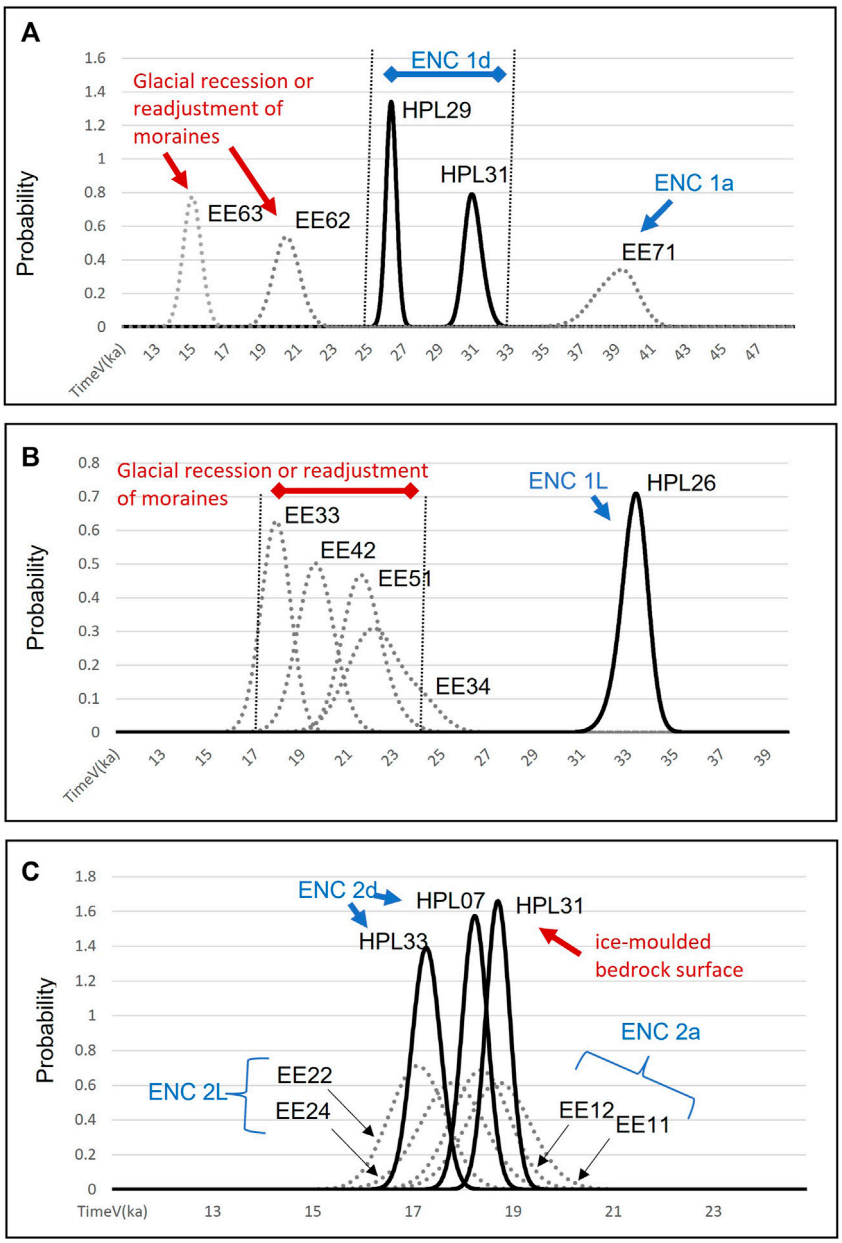

FIGURE 3 | Probability density function curves calculated from the exposure ^{10}Be ages. Age of samples obtained in this work in black solid curves and recalibrated from data of Zech et al. (2006) in gray segmented lines. **(A)** Moraines arcs of ENC 1 (25–40 ka) and glacial recession or readjustment of moraines. **(B)** Lateral moraines of ENC 1 (~33 ka) and glacial recession or readjustment of moraines (17–24 ka). **(C)** Moraine ridge and ice-molded bedrock surface of ENC2.

are much better preserved than the ones on the western side of the valley. The age of the lateral moraine agrees with the ages between 33–25 ka of inner-terminal moraine arc ENC 1d (**Figure 3**).

To recognize the age of the onset of deglaciation of glacial drift ENC 1 in the ERV, Zech et al. (2006) relied on exposure ages of lateral moraines that were developed as recessional positions of the glacier, recalibrated in this work to around 17–18 ka (EE22, EE24; **Figure 2**). This moraine ridge has been reinterpreted in this work as a lateral moraine related to the glacial advance of the tributary valley. The preservation of this ridge was only possible if the trunk valley was already deglaciated by that time. So, deglaciations of ENC 1 started at ~24 ka and finished before 18–17 ka. Indeed, this time span of deglaciation is consistent with our ice-molded bedrock age of 18.8 ± 0.7 ka (sample HPL-31) and suggests that the valley was almost completely deglaciated at that time.

Nonetheless, the time span for the deglaciation of ENC 1 coincides with the ages of boulders on moraines ENC 2a (EE11, EE12) obtained by Zech et al. (2006) a few kilometers down-valley

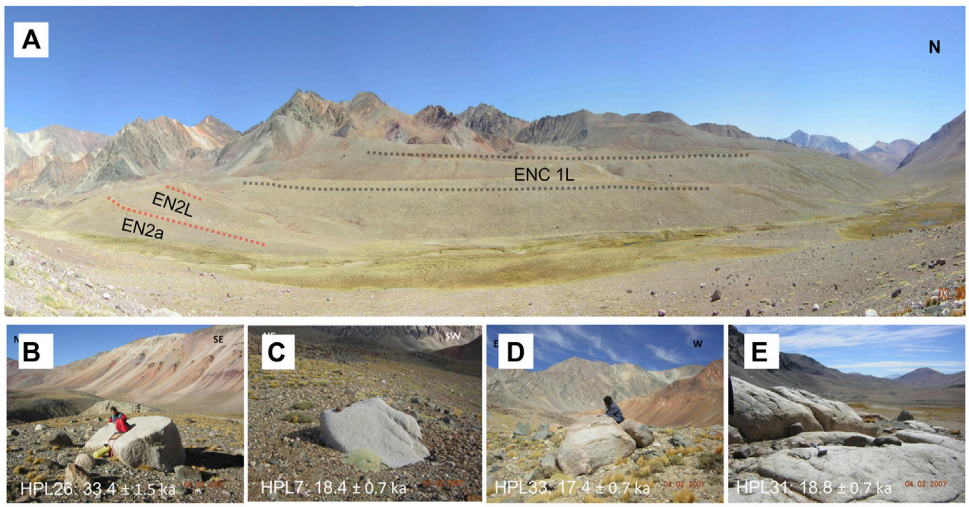

FIGURE 4 | Photographs of ^{10}Be sampling sectors. **(A)** Photograph toward the west taken from the location of sample toward the sequence of ENC 1L lateral moraines where Zech et al. (2006) dated four boulders between 17–24 ka (EE33, EE34, EE42 and EE51). **(B)** Photograph of sample HPL26 (lateral moraine of ENC 1L). **(C)** Photograph of sample HPL7 (recessional moraine ENC 2d). **(D)** Photograph of sample HPL33 (recessional moraine ENC 2d). **(E)** Photograph of ice-molded bedrock surface of valley bottom taken in the location of sample HPL31.

of the ice-molded bedrock samples (HPL-31; **Figure 2**). The ages of these two samples of moraine boulder is within 1 sigma and thus statistically the same (20–18 ka; **Figure 3B**). We interpret that the glacial advances of ENC 2a reached 9 km from the head of the valley, but the glacial erosion was not efficient to reset the nuclide concentrations of the ice-molded bedrock surface (sample HPL-31). In fact, ages of recessional moraine ridges ENC 2d (HPL07 and HPL33) suggest this glacial drift could be much thinner and retreat at 18–17 ka up the valley of the sampling site of HPL-31.

We suggest that valley deglaciation was completed by 18–17 ka. Thus, no major advances occurred in the ERV after 17 ka as proposed previously by Zech et al. (2017). Andean glaciations in the northern segment of the Atacama Desert were linked to CAPE humid events that occurred 16–10 ka (Quade et al., 2008). Any effect of this pluvial event on local glaciation was negligible in the valleys of the southern Atacama Desert, at least in the ERV (29°S), as already observed in the Cordon Doña Rosa (30°S; Zech et al., 2017). Deglaciation by 18 ka is a global warming signal at the start of the Heinrich Stadial Event 1 (HS1; 18–14.5 ka; Rasmussen et al., 2006), which is thought to play a direct role in the last glacial termination in the Andes through the high-latitude migration of the southern westerly winds and the CO_2 ventilation from the Southern Ocean (e.g., Denton et al., 2010).

DATA AVAILABILITY STATEMENT

The original contributions presented in the study are included in the article/Supplementary Material; further inquiries can be directed to the corresponding author.

AUTHOR CONTRIBUTIONS

AG: fieldwork, mapping and sampling, data interpretation, contextualization, and writing. RR: fieldwork, mapping and sampling, data interpretation, and contextualization. LP: fieldwork, mapping and sampling, and data interpretation. CA: contextualization and writing. GJ: contextualization and writing. CA: mapping and data interpretation. GJ: mapping and data interpretation.

FUNDING

This work was supported by the INNOVA-CORFO project (RR); the Basal Project of the Advanced Mining Technology Center financed by ANID Project AFB0004 (AG), and the FONDECYT grant # 1200935 (GJ).

REFERENCES

Ammann, C., Jenny, B., Kammer, K., and Messerli, B. (2001). Late Quaternary Glacier Response to Humidity Changes in the Arid Andes of Chile (18-29°S). *Palaeogeogr. Palaeoclimatol. Palaeoecol.* 172, 313–326. doi:10.1016/s0031-0182(01)00306-6

Balco, G., Stone, J. O., Lifton, N. a., and Dunai, T. J. (2008). A Complete and Easily Accessible Means of Calculating Surface Exposure Ages or Erosion Rates from 10Be and 26Al Measurements. *Quat. Geochronol.* 3, 174–195. doi:10.1016/j.quageo.2007.12.001

Bierman, P. R., Caffee, M. W., Davis, P. T., Marsella, K., Pavich, M., Colgan, P., et al. (2002). "4. Rates and Timing of Earth Surface Processes from In Situ-Produced Cosmogenic Be-10," in *Mineralogy & Geochemistry 50* (Washington: Mineralogical Society of America), 147–206. doi:10.1515/9781501508844-005

D'Arcy, M., Schildgen, T. F., Strecker, M. R., Wittmann, H., Duesing, W., Mey, J., et al. (2019). Timing of past glaciation at the Sierra de Aconquija, northwestern

Argentina, and throughout the Central Andes. *Quat. Sci. Rev.* 204, 37–57. doi:10.1016/j.quascirev.2018.11.022

Denton, G. H., Anderson, R. F., Toggweiler, J. R., Edwards, R. L., Schaefer, J. M., and Putnam, A. E. (2010). The Last Glacial Termination. *Science* 328, 1652. doi:10.1126/science.1184119

Grosjean, M., Geyh, M. A., Messerli, B., Schreier, H., and Veit, H. (1998). A Late-Holocene. *Holocene* 8 (4), 473–479. doi:10.1191/095968398677627864

Ivy-Ochs, S. (1996). *The Dating of Rock Surfaces Using* in Situ *Produced 10Be, 26Al and 36Cl, with Examples from Antarctica and the Swiss Alps*. Zürich, Switzerland: Unpublished PhD thesis.

Jenny, B., and Kammer, K. (1996). "Jungquartare Vergletscherung," in *Climate Change in Den Trockenen Anden*. Editors C. Ammann, B. Jenny, and K. Kammer (Bern, Switzerland: Geographica Bernensia), G46, 1–80.

Kohl, C. P., and Nishiizumi, K. (1992). Chemical Isolation of Quartz for Measurement of *In-Situ* -produced Cosmogenic Nuclides. *Geochimica Cosmochimica Acta* 56, 3583–3587. doi:10.1016/0016-7037(92)90401-4

Lal, D. (1991). Cosmic Ray Labeling of Erosion Surfaces: *In Situ* Nuclide Production Rates and Erosion Models. *Earth Planet. Sci. Lett.* 104, 424–439. doi:10.1016/0012-821x(91)90220-c

Latorre, C., Betancourt, J. L., and Arroyo, M. T. K. (2006). Late Quaternary Vegetation and Climate History of a Perennial River Canyon in the Río Salado Basin (22°S) of Northern Chile. *Quat. Res.* 65 (3), 450–466. doi:10.1016/j.yqres.2006.02.002

Martin, L., Blard, P.-H., Balco, G., Lave, J., Delunel, R., Lifton, N., et al. (2016). The CREp Program and the ICE-D Production Rate Calibration Database: a Fully Parameterizable and Updated Online Tool to Compute Cosmic-Ray Exposure Ages. *Quat. Geochronol.* 38, 25–49. doi:10.1016/j.quageo.2016.11.006

Martin, L. C. P., Blard, P.-H., Lavé, J., Braucher, R., Lupker, M., Condom, T., et al. (2015). *In Situ* cosmogenic 10Be Production Rate in the High Tropical Andes. *Quat. Geochronol.* 30, 54–68. doi:10.1016/j.quageo.2015.06.012

Muscheler, R., Beer, J., Kubik, P. W., and Synal, H.-A. (2005). Geomagnetic Field Intensity during the Last 60,000 Years Based on 10Be and 36Cl from the Summit Ice Cores and 14C. *Quat. Sci. Rev.* 24, 1849–1860. doi:10.1016/j.quascirev.2005.01.012

Nishiizumi, K., Imamura, M., Caffee, M. W., Southon, J. R., Finkel, R. C., and McAninch, J. (2007). Absolute Calibration of 10Be AMS Standards. *Nucl. Instrum. Methods Phys. Res. Sect. B Beam Interact. Mater. Atoms* 258, 403–413. doi:10.1016/j.nimb.2007.01.297

Quade, J., Rech, J. A., Betancourt, J. L., Latorre, C., Quade, B., Rylander, K. A., et al. (2008). Paleowetlands and Regional Climate Change in the Central Atacama Desert, Northern chile. *Quat. Res.* 69 (3), 343–360. doi:10.1016/j.yqres.2008.01.003

Rasmussen, S. O., Andersen, K. K., Svensson, A., Steffensen, J. P., Vinther, B. M., Clausen, H. B., et al. (2006). A new Greenland ice core chronology for the last glacial termination (1984e2012). *J. Geophys. Res. Atmos.* 111 (D6). doi:10.1029/2005jd006079

Rossel, K., Aguilar, G., Salazar, E., Martinod, J., Carretier, S., Pinto, L., et al. (2018). Chronology of Chilean Frontal Cordillera Building from Geochronological, Stratigraphic and Geomorphological Data Insights from Miocene Intramontane-Basin Deposits. *Basin Res.* 30, 289–310. doi:10.1111/bre.12221

Salazar, E., and Coloma, F. (2016). *Geología del Área Cerros de Cantaritos-Laguna Chica. Región de Atacama. Servicio Nacional de Geología y Minería, Carta Geológica de Chile, Serie Geología Básica*. Santiago, Chile 181, 171.

Stone, J. O. (2000). Air Pressure and Cosmogenic Isotope Production. *J. Geophys. Res.* 105, 23753–23759. doi:10.1029/2000JB900181

Uppala, S. M., KÅllberg, P. W., Simmons, A. J., Andrae, U., Bechtold, V. D. C., Fiorino, M., et al. (2005). The ERA-40 Re-analysis. *Q. J. R. Meteorological Soc.* 131, 2961–3012. doi:10.1256/qj.04.176

Valet, J.-P., Meynadier, L., and Guyodo, Y. (2005). Geomagnetic Dipole Strength and Reversal Rate over the Past Two Million Years. *Nature* 435, 802–805. doi:10.1038/nature03674

Veit, H. (1996). Southern Westerlies during the Holocene Deduced from Geomorphological and Pedological Studies in the Norte Chico, Northern Chile (27-33°S). *Palaeogeogr. Palaeoclimatol. Palaeoecol.* 123, 107–119. doi:10.1016/0031-0182(95)00118-2

Veit, H. (1993). Upper Quaternary Landscape and Clime Evolution in the Norte Chico (Northern Chile): an Review. *Mt. Res. Dev.* 13 (No. 2), 139–144. Mountain Geoecology of the Andes: Resource Management and Sustainable Development. doi:10.2307/3673631

Zech, R., Kull, C., and Veit, H. (2006). Late Quaternary Glacial History in the Encierro Valley, Northern Chile (29°S), Deduced from 10Be Surface Exposure Dating. *Palaeogeogr. Palaeoclimatol. Palaeoecol.* 234, 277–286. doi:10.1016/j.palaeo.2005.10.011

Zech, R., Zech, J., Kull, C., Kubik, P. W., and Veit, H. (2011). Early Last Glacial Maximum in the Southern Central Andes Reveals Northward Shift of the Westerlies at ~39 Ka. *Clim. Past.* 7, 41–46. doi:10.5194/cp-7-41-2011

Zech, J., Terrizzano, C., García-Morabito, E., Veit, H., and Zech, R. (2017). Timing and Extent of Late Pleistocene Glaciation in the Arid Central Andes of Argentina and Chile (22°-41°S). *Cuad. Investig. Geográfica* 43 (2), 697–718. doi:10.18172/cig.3235

Conflict of Interest: The authors declare that the research was conducted in the absence of any commercial or financial relationships that could be construed as a potential conflict of interest.

Publisher's Note: All claims expressed in this article are solely those of the authors and do not necessarily represent those of their affiliated organizations, or those of the publisher, the editors, and the reviewers. Any product that may be evaluated in this article, or claim that may be made by its manufacturer, is not guaranteed or endorsed by the publisher.

Copyright © 2022 Aguilar, Riquelme, Lohse, Cabré and García. This is an open-access article distributed under the terms of the Creative Commons Attribution License (CC BY). The use, distribution or reproduction in other forums is permitted, provided the original author(s) and the copyright owner(s) are credited and that the original publication in this journal is cited, in accordance with accepted academic practice. No use, distribution or reproduction is permitted which does not comply with these terms.